Comparison of Effective Permittivity Retrieval Methods of 3D-Printed Unit Cells for Dielectric Resonator Antenna Applications

Gaëtan Antoine, Bruno de Araujo, Romain Pascaud, Christophe Morlaas, Alexandre Chabory, Vincent Laquerbe, Gautier Mazingue

▶ **To cite this version:**

Gaëtan Antoine, Bruno de Araujo, Romain Pascaud, Christophe Morlaas, Alexandre Chabory, et al.. Comparison of Effective Permittivity Retrieval Methods of 3D-Printed Unit Cells for Dielectric Resonator Antenna Applications. 2023 17th European Conference on Antennas and Propagation (EuCAP), Mar 2023, Florence, Italy. pp.1-5, 10.23919/EuCAP57121.2023.10133663 . hal-04130869

HAL Id: hal-04130869
https://hal.science/hal-04130869

Submitted on 16 Jun 2023

HAL is a multi-disciplinary open access archive for the deposit and dissemination of scientific research documents, whether they are published or not. The documents may come from teaching and research institutions in France or abroad, or from public or private research centers.

L'archive ouverte pluridisciplinaire **HAL**, est destinée au dépôt et à la diffusion de documents scientifiques de niveau recherche, publiés ou non, émanant des établissements d'enseignement et de recherche français ou étrangers, des laboratoires publics ou privés.

Comparison of Effective Permittivity Retrieval Methods of 3D-Printed Unit Cells for Dielectric Resonator Antenna Applications

Gaëtan ANTOINE*†, Bruno DE ARAUJO*†, Romain PASCAUD*, Christophe MORLAAS†,
Alexandre CHABORY†, Vincent LAQUERBE‡, Gautier MAZINGUE§
*ISAE-SUPAERO, Université de Toulouse, Toulouse, FRANCE, gaetan.antoine@isae-supaero.fr
†ENAC, Université de Toulouse, Toulouse, FRANCE
‡Antenna Department, CNES, Toulouse, FRANCE
§ANYWAVES, Toulouse, FRANCE

***Abstract*—In this paper, three methods to retrieve the effective permittivity of 3D-printed unit cells for dielectric resonator antenna (DRA) applications are compared: Maxwell Garnett approximation (MGA), S-parameters method, and plane wave expansion method (PWEM). More specifically, three common topologies are studied: simple cubic (SC), body-centered cubic (BCC) and face-centered cubic (FCC). From numerical analyses, we explain which method is the most appropriate for designing a DRA using 3D-printed periodic unit cells.**

***Index Terms*—DRA, 3D printing, permittivity, unit cell.**

I. Introduction

Over the last 20 years, three-dimensional (3D) printing technologies have been developed to manufacture complex structures. Regarding antenna applications, horn [1], lens [2], reflector [3], and more recently dielectric resonator antennas (DRAs) [4]-[7], to cite a few, have already been 3D-printed.

DRAs have been studied since the 1980s [8] and are still investigated today. This is mainly due to their attractive features such as compact size, high gain, and high radiation efficiency [9]. 3D-printing of dielectric materials now opens up new possibilities in DRA design. Thus, the control of the shape [5][6] and dielectric constant (structuring layers [7] or unit cells [4]) of the DRA have been explored in the last 5 years. Most of the early works were using materials with dielectric constant up to 10. With new 3D-printing technologies being developed, materials with higher relative permittivity and low loss tangent can now be 3D-printed, as for example ceramics [10]. In particular, a DRA made up of periodic subwavelength unit cells mixing zirconia ($\varepsilon_r = 32.5$ and $\tan\delta = 1.9 \times 10^{-4}$ at 10 GHz) and air has been studied in [11]. The filling ratio and the anisotropy of the unit cells allowed to control the resonance frequency and the polarization of the DRA.

In order to design a DRA made up of periodic unit cells, a full-wave analysis can be performed. Most of the time, it is costly in time and computer resources. As it is well known that the behavior of a DRA is mainly determined by its dimensions and effective permittivity, an alternative solution is to analyze a single unit cell of the DRA in order to retrieve its effective permittivity. From a transcendental equation or by comparing with a solid model, this permittivity can be linked to the resonance frequency of the 3D-printed DRA.

Methods to relate the filling ratio of a unit cell, i.e. the percentage of dielectric in the unit cell volume, to its effective permittivity have been studied in previous works using either Maxwell Garnett approximation (MGA) [12][13], S-parameters method [12][14], or plane wave expansion method (PWEM) [13]. However, the size of the unit cells has always been chosen so that they are electrically-small to ensure a homogeneous macroscopic behavior. For high frequency applications, mechanical limits of 3D printer may no longer allow to comply with this assumption. Therefore, it appears interesting to evaluate the effective permittivity obtained with these methods for larger unit cells.

In this work, the behavior of the effective permittivity for different unit cells is studied using the three methods mentionned before. In Section II, unit cell topologies are presented. In Section III, the methods to retrieve the effective permittivity from simulations are detailed. In Section IV, numerical analyses are performed and the computing time and accuracy of the methods are compared. Finally, Section V concludes the paper.

II. Unit cell topology

For 3D-printed antennas made up of periodic subwavelength unit cells, cubic cells are the most commonly used among other types of Bravais lattices (tetragonal, monoclinic, orthorhombic, rhombohedral, hexagonal, or triclinic). It can be explained by the feasibility of such structures, the cubic being the easiest to manufacture.

Here, three common topologies for cubic unit cell are compared: simple cubic (SC), body-centered cubic (BCC), and face-centered cubic (FCC). They can be seen in Fig. 1, with the 3D-printed dielectric in blue and its spherical inclusions of air. A complementary topology can exist, reversing dielectric and air, but it requires additional dielectric cylinders between the dielectric spheres in that case in order to be printable.

Finally, the topologies are defined as follows:

This paper's copyright is held by the author(s). It is published in these proceedings and included in any archive such as IEEE Xplore under the license granted by the "Agreement Granting EurAAP Rights Related to Publication of Scholarly Work."
Authorized licensed use limited to: ISAE. Downloaded on June 16,2023 at 09:29:43 UTC from IEEE Xplore. Restrictions apply.

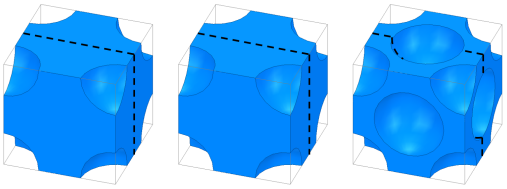

(a) Cubic unit cell

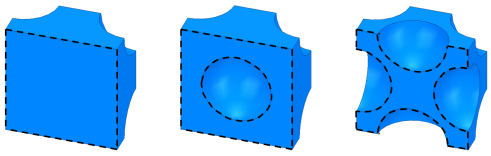

(b) Sectional view at dashed line

Fig. 1. From left to right: SC, BCC, and FCC cell.

- The SC lattice consists of one lattice point on each corner of the cube. Each atom at a lattice point is then shared equally between eight adjacent cubes, and the unit cell, therefore, contains a total of one atom (i.e., air inclusion).
- The BCC lattice has one lattice point in the center of the unit cell in addition to the corner points. It contains a total of two atoms per unit cell.
- The FCC lattice has lattice points on the faces of the cube in addition to the corner points. It contains a total of four atoms per unit cell.

III. Permittivity Retrieval Methods

In order to manufacture 3D-printed DRAs made up of periodic unit cells, dielectric behavior of the 3D-printed material has to be controlled. To find the resonance frequency associated with the fundamental mode of a dielectric resonator (DR), the most accurate way is to do an eigenmode analysis. For a DR made up of unit cells, it is also the most accurate method and it will be considered as our reference. However, for a DR with a large amount of unit cells, this method requires a lot of computing time and resources.

In order to reduce such requirements, a single unit cell of the DRA is often analyzed. The objective of this study is thus to compare three methods allowing to extract the effective permittivity of such unit cells. Note that all the simulations described in the following section are done with Ansys HFSS software.

A. Reference: Eigenmode analysis of a 3D-printed DR

At first, a DR over an infinite ground plane is considered for eigenmode analysis. Its permittivity is directly assigned on Ansys HFSS and it is lower than the one of the 3D-printed material. It is referred to as solid model and used as a reference as presented in Fig. 2a. More specifically, an eigenmode analysis of this solid model is performed to find the resonance frequency of its fundamental mode.

In a second step, an eigenmode analysis of the DR made up of periodic unit cells is performed. A DR made up of 64 BCC

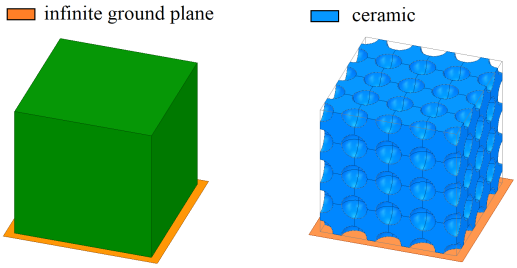

(a) Solid model (b) 64 BCC cells

Fig. 2. Simulation setup for the eigenmode analysis for the (2a) solid and for instance, (2b) 64 BCC cells models.

unit cells is presented in Fig. 2b as an example. The resonance frequency of its fundamental mode is identified by analyzing the electric and magnetic fields inside the DR. By varying the filling ratio of the unit cells, and thus, the effective permittivity of the DR, we set the computed resonance frequency of this mode at the same frequency as for the solid model.

This method can be time-consuming. However, it allows to design with a good accuracy a DR made up of periodic unit cells that has the same fundamental mode resonance frequency as a solid DR.

B. Method 1: Maxwell Garnett approximation

The theory behind the Maxwell Garnett approximation (MGA) is described in detail in [15]. The MGA describes the effective relative permittivity ε_{eff} of a dielectric material with relative permittivity ε_m filled with dielectric spheres with relative permittivity ε_i as

$$\varepsilon_{eff} = \varepsilon_m \frac{2\delta_i(\varepsilon_i - \varepsilon_m) + \varepsilon_i + 2\varepsilon_m}{2\varepsilon_m + \varepsilon_i - \delta_i(\varepsilon_i - \varepsilon_m)} \tag{1}$$

where δ_i is the volume fraction of the inclusions. In our case, ε_m refers to the ceramic dielectric constant, while $\varepsilon_i = 1$ for the air inclusions. Note that MGA method is expected to be valid at low volume fractions δ_i.

C. Method 2: S-Parameters method

This method relies on the Floquet simulation of a single cubic unit cell of side a_{uc}. As shown in Fig. 3, the simulation setup consists of a single cubic unit cell and a vacuum box four times the size of the unit cell along the z-direction. The vacuum box has periodic boundary conditions on the four side walls along the x- and y-axis and Floquet ports on the two faces along the z-axis. It provides a normal incident plane wave which polarization can be set.

The simulated S-parameters are used to retrieve the effective permittivity of the unit cell as a function of the frequency using the method described in [14]. In fact, the refractive index n and the impedance z of the unit cell are given by

$$z = \sqrt{\frac{(1+S_{11})^2 - S_{21}^2}{(1-S_{11})^2 - S_{21}^2}}, \tag{2}$$

This paper's copyright is held by the author(s). It is published in these proceedings and included in any archive such as IEEE Xplore under the license granted by the "Agreement Granting EurAAP Rights Related to Publication of Scholarly Work."
Authorized licensed use limited to: ISAE. Downloaded on June 16,2023 at 09:29:45 UTC from IEEE Xplore. Restrictions apply.

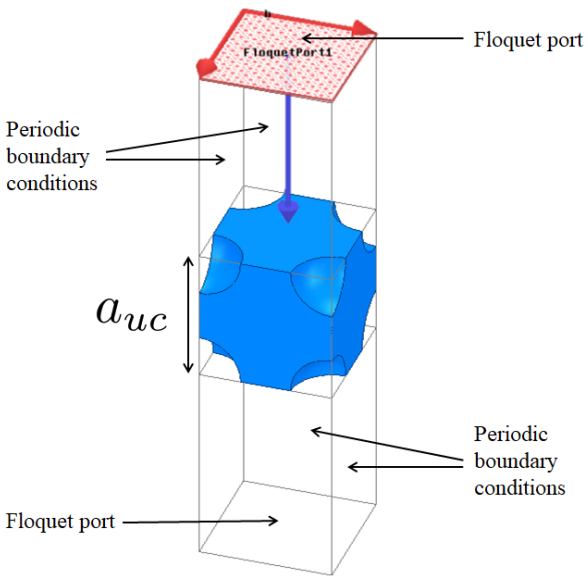

Fig. 3. Floquet simulation setup of a single BCC cell.

$$n = \frac{1}{k_0 a_{uc}} \cos^{-1}\left[\frac{1}{2S_{21}}(1 - S_{11}^2 + S_{21}^2)\right]. \quad (3)$$

The effective relative permittivity is finally computed using the ratio between the refractive index and the impedance of the unit cell

$$\varepsilon_{eff} = \frac{n}{z}. \quad (4)$$

This method is fast and easy to implement but it relies on several assumptions that restrict its applicability. One of them being that the unit cell must remain electrically-small. Commonly, effective permittivity retrieval of subwavelength unit cells is done with this method [11][12].

D. Method 3: Plane wave expansion method

The theory behind the plane wave expansion method (PWEM) is described in [16]. Only the eigenmode simulation setup and the exploitation of the data will be detailed hereafter.

Here, the simulation setup consists of a single unit cell with periodic boundary conditions along the x-, y-, and z-axis, as shown in Fig. 4.

The eigenmode simulation provides the frequencies associated with each eigenmode. Plotting the dispersion diagram, i.e., the frequency as a function of the wavenumber k, we can retrieve the effective relative permittivity with the following formula

$$\varepsilon_{eff} = \left(\frac{k\lambda_0}{2\pi}\right)^2, \quad (5)$$

where λ_0 is the free-space wavelength.

In this work, simulations will be done for the Γ-X part of the Γ-X-M-Γ-R-X irreductible Brillouin zone (IBZ) used for cubic

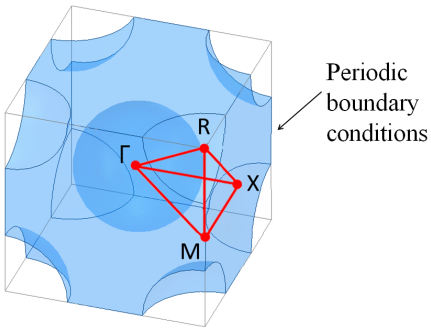

Fig. 4. Eigenmode simulation setup of a single BCC cell and its irreductible Brillouin zone (IBZ)

cells (see Fig. 4). This path is here considered because it is the same as for *method 2*. For future work, it can be interesting to study the anisotropy of the unit cell by analyzing other parts of the IBZ.

IV. Results

A. Optimization of filling ratio of the unit cells

A cubic DR of side equal to 16 mm, placed on an infinite ground plane, and using a dielectric with $\varepsilon_r = 15$ and $\tan\delta = 1.9 \times 10^{-4}$ has first been designed. The resonance frequency f_0 of its first two modes, $\mathrm{TE}^x_{\delta 11}$ and $\mathrm{TE}^y_{1\delta 1}$, is found to be $f_0 = 3.192$ GHz, i.e., a wavelength λ in the dielectric equal to 24.27 mm.

Three DR of the same dimensions, but made up of different number of unit cells, are then simulated with the eigenmode analysis described in Sec.III.A. They are structured as shown in Table I and Fig. 5 (BCC unit cells are used in this figure), considering 1 to 64 unit cells. However, considering Fig. 5c, one may wonder whether a single 16 mm unit cell can still be analyzed as a cubic DR.

TABLE I
UNIT CELLS SPECIFICATIONS FOR EACH DR AT $f_0 = 3.192$ GHZ

Number	a_{uc}	a_{uc}/λ
64	4 mm	1/6
8	8 mm	1/3
1	16 mm	1/1.5

Each DR has been optimized using SC, BCC, and FCC unit cells. As shown in Table II, the filling ratio of the unit cells has been chosen to obtain the same resonance frequency as for the reference solid model, namely 3.192 GHz.

One can observe that the filling ratio of the unit cells varies according to their topology, namely SC, BCC, or FCC. This is probably due to the spatial dispersion caused by their different degrees of isotropy. Moreover, as the size of a unit cell a_{uc} increases, its filling ratio also varies whatever the type of unit cell.

Although the resonance frequency is fixed to the required value of 3.192 GHz, it should be noted that it is not sufficient

This paper's copyright is held by the author(s). It is published in these proceedings and included in any archive such as IEEE Xplore under the license granted by the "Agreement Granting EurAAP Rights Related to Publication of Scholarly Work."
Authorized licensed use limited to: ISAE. Downloaded on June 16,2023 at 09:29:45 UTC from IEEE Xplore. Restrictions apply.

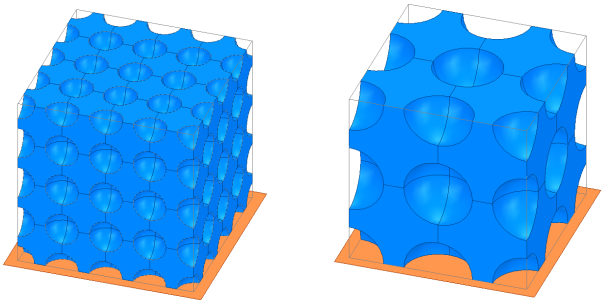

(a) $a_{uc} = 4$ mm (64 cells) (b) $a_{uc} = 8$ mm (8 cells)

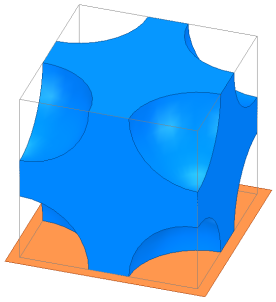

(c) $a_{uc} = 16$ mm (1 cell)

Fig. 5. DR made up of BCC unit cells.

TABLE II
UNIT CELLS FILLING RATIO AT $f_0 = 3.192$ GHz

	filling ratio		
a_{uc}	SC	BCC	FCC
4 mm	47.11%	47.48%	47.54%
8 mm	50.21%	48.51%	48.42%
16 mm	48.81%	54.58%	52.37%

to guarantee the same antenna behavior as the reference DRA at the end. For instance, another relevant parameter of the antenna performance of a DRA is its quality factor Q. As can be seen in Fig. 6, in the case of DRs made up of periodic unit cells, the value of Q varies with the size and topology of the unit cell. Therefore, the same electromagnetic properties as for the reference antenna cannot be assumed. Further full wave simulation of complete DRA are thus required.

B. Computing time

Simulations of DRs made up of unit cells have been performed on a PC with 256 Go of RAM and a processor Intel®Xeon®CPU E5-2690.

Considering for instance a DR made up of 64 BCC unit cells, i.e., $a_{uc} = 4$ mm, the computing time necessary to obtain the resonance frequencies of the DR and to run *method 2* and *method 3* are given in Table III.

From Table III, it can be seen that the eigenmode simulation of a full DR made up of unit cells can be extremely time-consuming. It shows why it can be useful to employ *method 2* or *method 3* in order to derive the permittivity of the DR through the permittivity of a single unit cell.

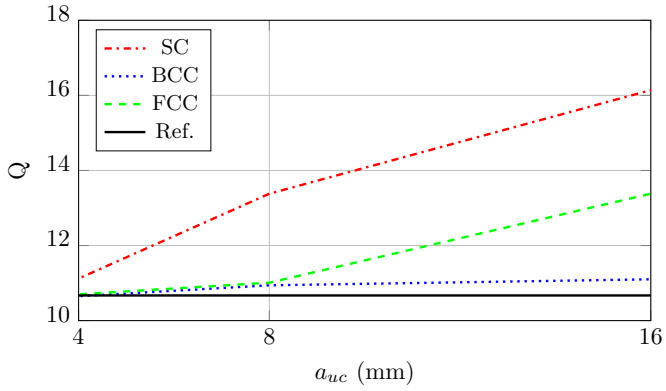

Fig. 6. Q factor of the DR as a function of a_{uc} for the different topologies of unit cells.

TABLE III
COMPARISON OF COMPUTING TIME BETWEEN THE DIFFERENT METHODS FOR A 4 MM BCC CELL

Type of method	Computing time (hh:mm:ss)
Reference	03:07:26
Method 2	00:02:46
Method 3	00:06:17

C. Comparison between methods

The results of the simulations are reported in Table IV. The effective permittivity ε_{eff} of the unit cell at the resonance frequency $f_0 = 3.192$ GHz of the DR, and the error in percentage from the reference value, namely $\varepsilon_r = 15$, are given for each method, cell topology and size.

Values for the computed effective permittivity are very close between *method 2* and *method 3* for BCC and FCC unit cells when a_{uc} is equal to 4 mm. The smallest SC unit cell indicates a trend: *method 2* does not give accurate results for every unit cell topology. This trend is confirmed with 8 mm unit cells, where the permittivity of the SC topology at the resonance frequency of the DR is equal to 19.07 instead of being close to 15 as it is the case in *method 3*.

When a_{uc} is too close to the wavelength, dispersion effects may cause the results of *method 2* to be unreliable regardless of the topology of the unit cell. The results of *method 2* are then noted N/A (not applicable). On the contrary, *method 3* is still efficient for unit cell dimension around the wavelength.

To conclude, the PWEM remains the most accurate method whatever the unit cell size in our example.

V. CONCLUSION

In this paper, a comparison between three methods to extract the effective permittivity of periodic unit cells for 3D-printed DRA has been proposed.

When designing a DRA made up of periodic unit cells mixing dielectric and air, extracting its effective permittivity

This paper's copyright is held by the author(s). It is published in these proceedings and included in any archive such as IEEE Xplore under the license granted by the "Agreement Granting EurAAP Rights Related to Publication of Scholarly Work."
Authorized licensed use limited to: ISAE. Downloaded on June 16,2023 at 09:29:45 UTC from IEEE Xplore. Restrictions apply.

TABLE IV
COMPARISON OF ε_{eff} AT $f_0 = 3.192$ GHZ FOR DIFFERENT a_{uc}

$a_{uc} = 4$ mm (λ/6)	*method 1* MGA		*method 2* S-parameters		*method 3* PWEM	
unit cell top.	ε_{eff}	error	ε_{eff}	error	ε_{eff}	error
SC	14.60	2.67%	15.48	3.20%	15.01	0.07%
BCC	14.49	3.40%	14.99	0.07%	15.03	0.20%
FCC	14.47	3.53%	15.04	0.27%	14.98	0.13%

$a_{uc} = 8$ mm (λ/3)	*method 1* MGA		*method 2* S-parameters		*method 3* PWEM	
unit cell top.	ε_{eff}	error	ε_{eff}	error	ε_{eff}	error
SC	13.65	9.00%	19.07	27.13%	15.14	0.93%
BCC	14.17	5.53%	15.03	0.20%	15.08	0.53%
FCC	14.20	5.33%	15.23	1.53%	14.92	0.53%

$a_{uc} = 16$ mm (λ/1.5)	*method 1* MGA		*method 2* S-parameters		*method 3* PWEM	
unit cell top.	ε_{eff}	error	ε_{eff}	error	ε_{eff}	error
SC	14.08	6.13%	N/A	N/A%	15.80	5.33%
BCC	12.35	17.67%	N/A	N/A%	15.57	3.80%
FCC	13.00	13.33%	N/A	N/A%	14.78	1.47%

can be very time-consuming depending on the number of cells. For this reason, three methods allowing this extraction using a single unit cell have been compared.

The S-parameters method is commonly used in the literature but has assumptions about the size of the unit cell that restricts its applicability for high frequency applications. However, the PWEM remains accurate for larger unit cells, even close to the wavelength, and no matter the cell topology.

Future works include studying the results provided by these methods on the spatial and frequency dispersion behavior of cubic unit cells.

ACKNOWLEDGMENT

The authors would like to thank the French Agency for Innovation of Defense (Agence de l'Innovation de Défense, AID) and the French National Center of Space Studies (Centre Nationale d'Etudes Spatiales, CNES) for the funding.

REFERENCES

[1] J-C. S. Chieh, B. Dick, S. Loui, and J. D. Rockway, "Development of a Ku-band corrugated conical horn using 3-D print technology," IEEE Antennas and Wireless Propagation Letters, vol. 13, pp. 201-204, 2014.

[2] H. Yi, S-W. Qu, K-B. Ng, C. H. Chan, and X. Bai, "3-D printed millimeter-wave and terahertz lenses with fixed and frequency scanned beam," IEEE Transactions on Antennas and Propagation, vol. 64, no. 2, pp. 442-449, Feb. 2016.

[3] P. Nayeri, M. Liang, R. A. Sabory-Garcia, M. Tuo, F. Yang, M. Gehm, H. Xin, and A. Z. Elsherbeni, "3D printed dielectric reflectarrays: Low-cost high-gain antennas at sub-millimeter waves," IEEE Transactions on Antennas and Propagation, vol. 62, no. 4, pp. 2000-2008, Apr. 2014.

[4] Z-X. Xia, K. W. Leung, and K. Lu, "3-D-printed wideband multi-ring dielectric resonator antenna," IEEE Antennas and Wireless Propagation Letters, vol. 18, no. 10, pp. 2110-2114, Oct. 2019.

[5] V. Basile, M. Grande, V. Marrocco, D. Laneve, S. Petrignani, F. Prudenzano, and I. Fassi, "Design and manufacturing of super-shaped dielectric resonator antennas for 5G applications using stereolithography," IEEE Access, vol. 8, pp. 82929-82937, 2020.

[6] F. P. Chietera, R. Colella, and L. Catarinucci, "Dielectric resonators antennas potential unleashed by 3D printing technology: A practical application in the IoT framework," Electronics, vol. 11, no. 1, pp. 64, 2022.

[7] Z-X. Xia and K. W. Leung, "3-D-printed wideband circularly polarized dielectric resonator antenna with two printing materials," IEEE Transactions on Antennas and Propagation, vol. 70, no. 7, pp. 5971-5976, Jul. 2022.

[8] S. Long, M. McAllister, and L. Shen, "The resonant cylindrical dielectric cavity antenna," IEEE Transactions on Antennas and Propagation, vol. 31, no. 3, pp. 406-412, May 1983.

[9] A. Petosa, *Dielectric Resonator Antenna Handbook*, 2007.

[10] G. Mazingue, M. Romier, and N. Capet, "3D printed ceramic low-profile GNSS antenna for SmallSats," 2020 50th European Microwave Conference (EuMC), pp. 460-462, 2021.

[11] C. D. Morales, C. Morlaas, A. Chabory, R. Pascaud, M. Grzeskowiak, and G. Mazingue, "3D-printed ceramics with engineered anisotropy for dielectric resonator antenna applications," Electronics Letters, vol. 57, no. 18, pp. 679-681, Aug. 2021.

[12] G. Mazingue, B. Byrne, M. Romier, and N. Capet, "3D printed ceramic antennas for space applications," 2020 14th European Conference on Antennas and Propagation (EuCAP), pp. 1-5, Mar. 2020.

[13] S. P. Hehenberger, A. P. T. Adithyababu, and S. Caizzone, "Effective permittivity measurement of 3D-printed dielectric crystals," 2022 16th European Conference on Antennas and Propagation (EuCAP), pp. 1-5, Mar. 2022.

[14] A. B. Numan and M. S. Sharawi, "Extraction of material parameters for metamaterials using a full-wave simulator [education column]," IEEE Antennas and Propagation Magazine, vol. 55, no. 5, pp. 202-211, Oct. 2013.

[15] T. C. Choy, *Effective Medium Theory: Principles and Applications*, International Series of Monographs on Physics, OUP Oxford, pp. 5-12, 2015.

[16] R. C. Rumpf and J. Pazos, "Synthesis of spatially variant lattices," Optics Express, vol. 20, pp. 15263-15274, 2012.

This paper's copyright is held by the author(s). It is published in these proceedings and included in any archive such as IEEE Xplore under the license granted by the "Agreement Granting EurAAP Rights Related to Publication of Scholarly Work."
Authorized licensed use limited to: ISAE. Downloaded on June 16,2023 at 09:29:45 UTC from IEEE Xplore. Restrictions apply.